Effects of Multiwalled Carbon Nanotubes on the Shear-Induced Crystallization Behavior of Poly(butylene terephthalate)

Gaurav Mago,[†] Frank T. Fisher,[†] and Dilhan M. Kalyon*[,‡]

Department of Mechanical Engineering, Stevens Institute of Technology, Hoboken, New Jersey 07030, and Highly Filled Materials Institute and Department of Chemical, Biomedical and Materials Engineering, Stevens Institute of Technology, Hoboken, New Jersey 07030

Received April 21, 2008; Revised Manuscript Received September 5, 2008

ABSTRACT: The effects of the incorporation of multiwalled carbon nanotubes (MWNT) with a diameter range of 10−30 nm on the shear-induced crystallization behavior of poly(butylene terephthalate) (PBT) were investigated under myriad shearing and loading conditions employing principally the small-amplitude oscillatory shear flow. Upon shearing, the presence of MWNTs leads to the crystallization of the PBT nanocomposites at temperatures that are higher than the crystallization temperature of unfilled PBT. The Avrami analysis of the shear-induced crystallization data of PBT nanocomposite samples indicated that the kinetics of the crystallization depend on both the temperature and the concentration of the MWNTs. When the MWNTs were replaced with ∼70 μm graphite particles at similar volume loading levels the crystallization behavior of the PBT/graphite suspension samples did not differ from that of pure PBT. These findings emphasize that one primary mechanism associated with the significant changes in the mechanical properties observed upon the compounding of nanoparticles into various semicrystalline polymers is the change in the crystallization behavior of the polymer as affected by the presence and the concentration of the nanoparticles and the associated changes in the microstructural distributions of the nanocomposite.

1. Introduction

Poly(butylene terephthalate) (PBT) is a semicrystalline thermoplastic that is widely used in various applications including those in electronics and telecommunication equipment, computers, electrical connectors and automotive parts in both "under the hood" and exterior applications. PBT has a glass transition temperature of around 45 °C and exhibits a relatively fast crystallization rate. Since it is considered to have a relatively broad processing window (i.e., PBT can be shaped using extrusion or molding processes over a wide range of geometries and operating conditions), it is an important candidate for being compounded with various nanoparticles to further broaden its utility. Significant improvements in ultimate properties have been observed to occur upon the incorporation of various types of nanoparticles into commodity and engineering polymers.[1−8] In particular, multiwalled carbon nanotubes (MWNTs) have stimulated great interest in the nanocomposites field due to their relatively high surface to volume and aspect ratios, and their relatively low density, high tensile modulus, and high electrical conductivity.[9]

A number of advances have recently been made in the solvent-based or solution-based processing of polymer nanocomposites. However, such processing methods are not eco-friendly and generally require the use of expensive and toxic solvents. The solventless compounding of nanoparticles directly into a polymer melt removes the negative environmental impact associated with solvent based processing and reduces the cost of manufacturing. Such melt compounding requires the application of relatively high shearing stresses repeatedly to disperse particles and to generate composition uniformity and is accomplished using twin screw extruders, kneaders, intensive batch mixers and shear roll mills.[10−19]

The ultimate properties of processed articles are intimately linked to the microstructural distributions that are generated during the processing and shaping stages. The thermo-mechanical history associated with the crystallization process during solidification has a particularly significant effect on the development of crystallinity and density distributions observed upon solidification.[20,21] To gain insight into the development of crystallinity under quiescent conditions, differential scanning calorimetry is generally used in conjunction with Avrami analysis to characterize the crystallization kinetics of various semicrystalline polymers, including PBT,[22] PEEK,[23,24] PE,[25] and *s*-PP.[26]

In earlier studies of the development of the mechanical and other ultimate properties of nanocomposites, the primary focus was on the "reinforcement" aspect of the nanoparticles associated with their very high surface to volume and aspect ratios.[27] However, it is also clear that the presence of the nanoparticles can alter the development of crystallinity within the nanocomposite, since the nanoparticles can act as heterogeneous nuclei to increase the nucleation rate, leading to an increase of crystallinity and decrease of crystallite sizes. Such changes in crystallinity as well as changes in the dynamics of the crystallization process have been observed with MWNTs, typically with the crystallization occurring under quiescent conditions.[28−31] However, realistic nanocomposites are not manufactured under quiescent conditions but rather are derived from a complex thermo-mechanical history during which the macromolecules undergo relatively high rates of shear and extension followed by rapid quenching. The complexities of the thermo-mechanical histories experienced by unfilled macromolecules[32−39] and macromolecules filled with micrometer-sized particles during their processing, and the resulting changes in structure and ultimate properties, are well documented and suggest the need to consider the effects of the thermal and deformation history on the development of various microstructural distributions within polymer nanocomposites as well.[11−15]

Detailed studies which link the crystallization kinetics of the polymeric binders of nanocomposites to their rheological behavior on one hand and to their processability on the other

* Corresponding author. E-mail: dilhan.kalyon@stevens.edu.
[†] Department of Mechanical Engineering, Stevens Institute of Technology.
[‡] Highly Filled Materials Institute and Department of Chemical, Biomedical and Materials Engineering, Stevens Institute of Technology.

10.1021/ma8008838 CCC: $40.75
Published on Web 10/14/2008

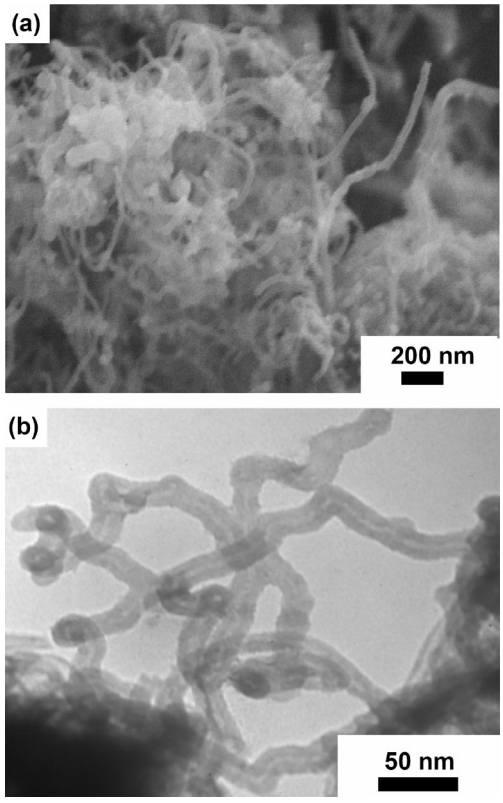

Figure 1. Multiwalled carbon nanotubes: (a) SEM image; (b) TEM image.

are currently lacking. For example, it is known that the application of a shear stress to a polymer melt at temperatures which are in the vicinity of the crystallization temperature leads to the shear-induced orientation of the macromolecules, thus reducing the entropy of the melt and leading to flow-induced crystallization.[40−46] However, it is not clear what role the presence of the nanoparticles would play during such shear-induced crystallization. Development of rheological characterization-based methods to analyze shear-induced crystallization and the application of such methods would serve to elucidate the role that the nanoparticle phase would play during shear-induced crystallization. In this study, the time, temperature and deformation rate dependencies of the dynamic properties, i.e., moduli collected using oscillatory-shear in the linear viscoelastic range, were used to shed light on the shear-induced crystallization of MWNT-PBT nanocomposites, with both pure PBT samples and PBT reinforced with micrometer-sized graphite particles used as control samples. The surface to volume ratio of the rigid particles (MWNTs in the 10−30 nm range and 70 μm sized graphite) and their concentrations were employed as the major parameters of the study.

2. Experimental Section

2.1. Materials. The PBT used as the binder was obtained as pellets (trade name: Celanex-2001 EF-NAT) from Ticona Polymers (North Carolina), with a density of 1.31 g/cc and melt index of 7.2 g/10 min. PBT pellets were dried in a vacuum oven at 125 °C for 4 h to reduce their moisture content prior to use. The zero shear viscosity of PBT was determined to be 680 Pa.s at 245 °C (frequency sweep experiments conducted at 245 °C and 10% strain). The MWNTs (trade name: MWNT-A-P) were purchased from Sunnano (China). The diameter and the length ranges of the MWNTs were reported by the manufacturer to be 10−30 nm and 1−10 μm, respectively. To examine the size and shape distributions of the MWNTs a LEO 1550 scanning electron microscope (SEM) operated at 15kV was used. Figure 1a shows a scanning electron micrograph of the as-received MWNTs. Transmission Electron Microscope (TEM) analysis of MWNTs was carried out using a JEOL1010. Figure 1b shows a TEM micrograph of the MWNTs. To study the state of the dispersion of the MWNTs in the PBT matrix, thin sections (90 nm thickness) were microtomed using an LKB ultramicrotome and analyzed via TEM. Graphite powder (grade: A-60) was obtained from Asbury Mills, NJ, and was used as a control to probe the effects of the very high surface to volume ratio of the nanotubes versus the larger graphite particles. The graphite powder exhibited an average particle size of 70 μm, surface area of 3 m^2/g and density of 2.5 g/cm^3 (information available from Asbury Mills, NJ).

2.2. Melt Compounding of Nanocomposite Samples. MWNT-PBT nanocomposites were melt-compounded in batch using a Haake torque rheometer with a 300 mL intensive mixing head. The torque rheometer is an intensive mixer (a mini-Banbury mixer) with two counter-rotating and fully intermeshing rotors. It has the capability of measuring the time-dependent torque and hence the specific energy input during the mixing process. Mixing of MWNTs with PBT was carried at 245 °C for 8 min at 32 rpm at a degree of fill of about 70% (the ratio of the volume of the mixture over the volume of the mixing head available for flow). The mixing time was selected on the basis of the observed variation of the torque imposed on the rotating blades of the mixer versus time. The mixing was stopped at the point where a steady value of the torque could be obtained. This corresponds to about 8 min. The temperature and the blade rotational speed were selected on the basis of the typical processing conditions (temperature and shear rates) used in the industrial compounding of PBT. The loading levels of the nanocomposites were 0.5, 1 and 2.0% (by volume) of MWNTs. The corresponding wt % loadings of MWNTs are 0.57, 1.14 and 2.28%. Graphite powder was also melt-mixed with PBT under the similar conditions to provide 0.5, 1, and 2.0% (by volume) composites (hereafter called as 0.5% GR-PBT, 1% GR-PBT and 2% GR-PBT). Furthermore, sample of pure PBT was also subjected to a similar processing history. After mixing the samples were removed and sealed within two polyethylene bags. Specimens were compression molded using a Carver hot press at 245 °C for 5 min, followed by rheological characterization.

To analyze the dispersion of MWNTs within the PBT nanocomposites, samples were submerged in liquid N_2 for 3−4 min followed by fracturing, upon which the fractured surfaces were analyzed using SEM. Figure 2 shows SEM micrographs of the fracture surfaces obtained upon cryofracturing. Such images of the nanocomposite fracture surfaces indicate a relatively homogeneous dispersion of the MWNTs in the PBT nanocomposites. To further confirm acceptable dispersion of the MWNTs within the PBT matrix, TEM imaging was also conducted (see representative image in Figure 3). In such TEM images a number of MWNTs of varying length can be observed. The varying lengths are attributed to both the breaking/curling of MWNTs during the microtoming process as well as the distortion of the projected nanotube image as observed in TEM due to the orientation of the nanotube within the nanocomposite with respect to the electron beam. Noteworthy in such images is the general lack of visible large clusters or bundles of MWNTs within the sample, further suggesting adequate dispersion of the MWNTs within the nanocomposites.

For further microstructural analysis the PBT and nanocomposite samples were also studied using polarized light microscopy with thin microtomed slices (cut thickness: 2−4 μm) placed between two glass slides, and examined using a Nikon Optiphot 2-POL microscope. In addition, nanocomposite samples were etched in fuming nitric acid for 30 min at room temperature to enable the observation of the crystalline morphology of the sample under SEM. After etching the nanocomposite samples were washed with deionized water followed by drying in a vacuum oven for 24 h at room temperature prior to optical microscopy and scanning electron microscopy.

2.3. Rheological Characterization. The linear viscoelastic material functions of PBT, MWNT-PBT and graphite-PBT nanocomposites were characterized by employing small-amplitude

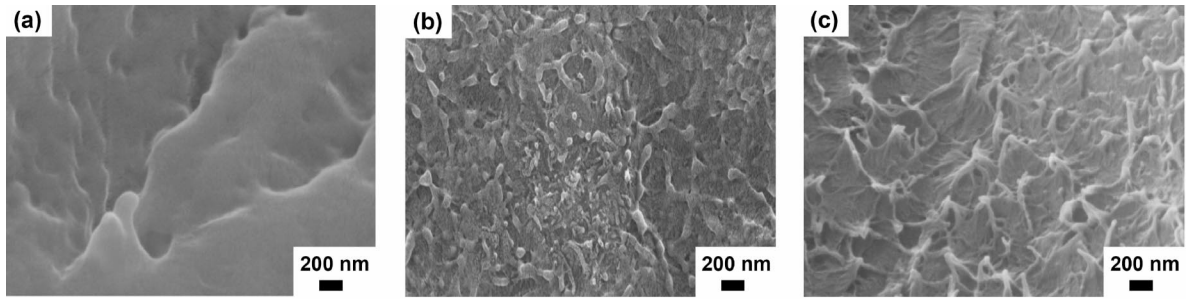

Figure 2. SEM of cryofractured samples: (a) pure PBT, (b) 0.5% MWNT-PBT, and (c) 2% MWNT-PBT nanocomposites.

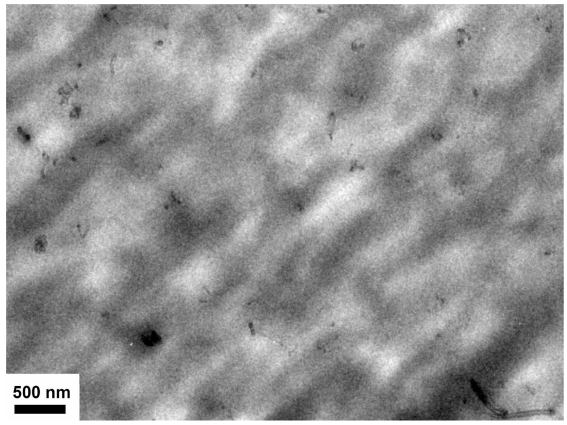

Figure 3. Representative TEM image of 2% MWNT-PBT nanocomposite sample.

oscillatory shear using an ARES (Advanced Rheometric Expansion System) rheometer with a force rebalance transducer (2K-FRTN1) available from TA Instruments. The actuator of the ARES is a *dc* servomotor with a shaft supported by an air bearing with an angular displacement range of 0.05−500 mrad. The temperature of the environmental chamber of the rheometer is controllable within ± 0.1 °C. The test fixtures consisted of stainless steel disks with a diameter of 25 mm. Prior to the oscillatory shear, the samples were heated to 245 °C after which the final gap between the two disks was set followed by the trimming of the excess specimen protruding out of the gap. During the preliminary stages of the investigation various gaps in the 0.5 to 1.5 mm range were used. Generally, the gap thickness selected becomes very important under conditions in which the wall slip of the suspension sample is appreciable, since the wall slip behavior of a suspension would be a function of the surface to volume ratio of the rheometer, i.e., would be a function of the reciprocal gap thickness.[47−52] All of the experiments reported here were carried out at a constant gap thickness of 0.7 mm. Upon loading and temperature equilibration, the specimens were allowed to relax for 5 min, upon which they were cooled to the targeted test temperature at which the dynamic properties were characterized as a function of time. The magnitude of the strain amplitude and the frequency were altered systematically in different runs. For each condition tested confidence intervals, determined according to Student's *t*-distribution obtained on the basis of at least four samples per condition, are reported. A fresh sample was used for each experiment. The samples were collected after shearing so that their degree of crystallinity as a function of time during the shear-induced crystallization process could be determined via differential scanning calorimetry as outlined in section 2.5.

2.4. Tensile Properties. To evaluate the effect of crystallinity on mechanical properties, tensile properties of the PBT and 2% MWNT-PBT nanocomposite samples were characterized. Pure PBT samples were annealed in a vacuum oven at 200 °C for 2 and 5 h, to obtain samples with different degrees of crystallinity. The tensile properties were characterized using a Rheometric System Analyzer (RSA-III, TA Instruments), at a constant extension rate of 0.001 mm/s at room temperature. The rectangular sample dimensions were 25 × 5 × 0.7 mm. A new sample was used for each tensile test.

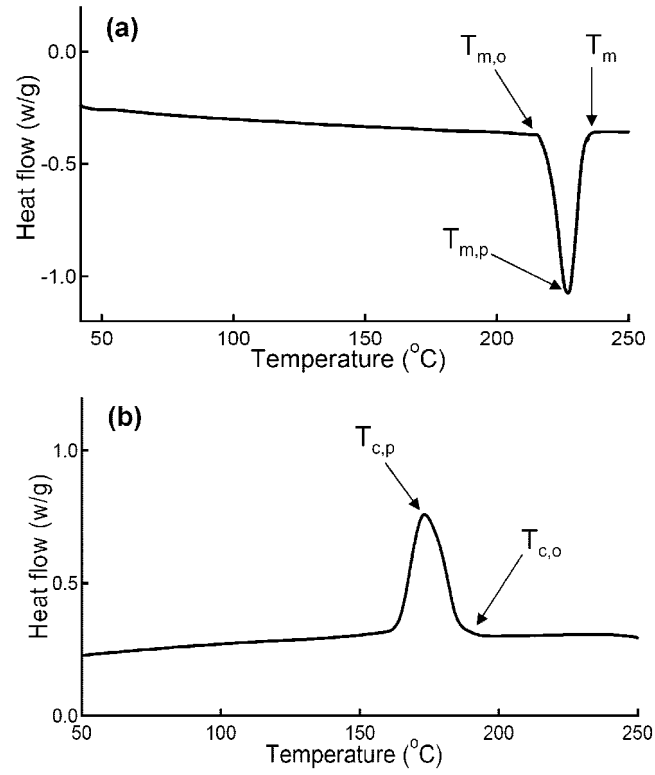

Figure 4. Typical DSC scans of pure PBT upon (a) heating and (b) cooling at 10 °C/min.

2.5. Thermal Analysis. Differential scanning calorimetry (DSC) studies were conducted using a TA Instruments (New Castle, DE) DSC model Q1000 focusing on the specimens of pure PBT and PBT nanocomposites. During differential scanning calorimetry the specimens (sample size was around 10 mg) were ramped from 25 to 255 °C and kept at 255 °C for ten minutes and were then cooled back down to 25 °C. The heating and cooling rates were 10 °C/min. Typical DSC scans of pure PBT obtained upon heating and cooling are shown in Figure 4. The temperatures associated with the onset of the melting, $T_{m,o}$, the melting temperature T_m (defined as the highest temperature at which the last trace of crystallinity disappears during heating), and the crystallization onset temperature, $T_{c,o}$ (the highest temperature at which the crystallization process is onset, while the sample is being cooled down from 255 °C) are shown in the Figure 4. The nominal melting temperature ($T_{m,p}$) was defined as the peak of the melting endotherm during heating from 25 to 255 °C, and the nominal crystallization temperature ($T_{c,p}$) was defined as the peak of the crystallization exotherm upon cooling from 255 to 25 °C. The degree of crystallinity, X_c (i.e., the weight fraction crystallinity), was determined as the ratio of the integrated heat of fusion value of the sample over the heat of fusion of purely crystalline PBT, i.e., 140 J/g:[53]

$$X_c = \frac{\Delta H_m \times 100}{\Delta H_{100\%,crystalline}} \quad (1)$$

3. Results and Discussion

3.1. Thermal Characterization of PBT and PBT Nanocomposites. The effects of MWNTs on the crystallization behavior of PBT and nanocomposites of PBT under quiescent conditions were analyzed via nonisothermal DSC experiments as reported in Table 1. The results of crystallization under quiescent conditions obtained with DSC suggest that even in the absence of shear and at relatively minor concentrations of MWNTs, there are noteworthy changes in the dynamics of the crystallization process and the ultimate crystallinity values attained for PBT upon the incorporation of the MWNTs. Overall, there are only modest reductions, i.e., 2−6 °C in the melting temperatures with 0.5 to 2% by volume MWNTs. On the other hand, there are significant increases in the crystallinity upon the incorporation of the MWNTs; for example, the degree of crystallinity under constant cooling rate increases from 20.7% for pure PBT to 24.5% for PBT incorporated with 2% by volume MWNTs.

The significant increase in crystallinity is accompanied by major increases in the crystallization temperatures of PBT observed upon the incorporation of the MWNTs. For example, the temperature at which crystallization is onset, $T_{c,o,}$ increases by about 22 °C and the peak crystallization temperature, $T_{c,p}$, increases by 29.4 °C with only 0.5% by volume of MWNTs (Table 1). Additional increases in the concentration of the MWNTs generate only modest additional increases in the crystallization temperature.

These DSC results obtained for crystallization under quiescent conditions that suggest that the crystallization temperature of the polymer is significantly affected upon the incorporation of the nanoparticles are in agreement with the quiescent crystallization results obtained for polypropylene (PP) incorporated with SWNTs.[54] Similar changes in melting behavior under quiescent conditions have also been observed for PP incorporated with MWNTs[55] and PLLA compounded with nanoclays.[56] The observed increase of the crystallinity of the PBT upon the incorporation of the MWNTs observed here is again in agreement with the increase of crystallinity of other polymers incorporated with nanoparticles i.e., poly(etheretherketone)-(PEEK) with carbon nanofibers[57] and poly(vinyl alcohol)[58] and poly(ethylene-2,6-naphthalate) with MWNTs.[59] The significant increases in various ultimate properties, including the enhancement of mechanical and permeability properties, are generally considered to be linked to the very high surface to volume ratios of nanoparticles in general[9,29]and MWNTs in particular.[29,60] However, the significant increases of crystallinity upon the incorporation of relatively modest concentrations of MWNTs (as low as 0.5% by volume) could be an additional major contributing factor giving rise to the significant property enhancements of polymeric nanocomposites. Further support to this hypothesis is provided below in the discussion of the shear-induced crystallization behavior of PBT and its nanocomposites, where it will be shown that additional significant gains in crystallinity are obtained upon the shear-induced crystallization of the PBT in the presence of carbon nanotubes.

3.2. Effect of MWNTs on Shear-Induced Crystallization Behavior of PBT. Linear viscoelastic material functions are very sensitive to structural changes in the polymer melt and can provide information on changes in the physicochemical properties of the polymer during deformation. For example, for thermally sensitive polymer melts, an irreversible decrease in viscosity with time at a constant shear rate suggests the possibility of thermal degradation of polymer molecules, whereas an irreversible increase in viscosity with time suggests the possibility of chemical cross-linking between polymer molecules. Both thermal degradation and chemical cross-linking are irreversible in the rheological responses they generate. On the other hand, sudden increases in the linear viscoelastic properties with time during shearing under constant deformation conditions at temperatures which are greater than the quiescent crystallization temperature of the pure melt suggest the flow-induced crystallization of the polymer melt upon shearing. Thus, upon shear-induced crystallization unbounded monotonic increases in the storage moduli (G'), loss moduli (G''), and magnitude of complex viscosity $|\eta^*|$ with time are observed.[61−63] Pennings and co-workers have documented that the morphology of such crystals formed upon shearing is typically of the "shish kebab" type and is thus very different than the typical row-nucleated and spherulitic morphologies that are generally observed under quiescent crystallization from the melt.[64−67]

Figure 5 shows the typical shear-induced crystallization results obtained for the dynamic properties versus time for PBT, MWNT-PBT nanocomposites and graphite-PBT composite samples collected at a constant frequency of 5 rps and 1% strain amplitude at 215 °C. As shown in Figure 5a, an increase in G′ with time was observed for MWNT-PBT nanocomposites that was not observed for pure PBT and graphite-PBT under similar conditions. This indicates a sharp increase in the crystallization rate due to the incorporation of MWNTs into PBT. Furthermore, the crystallization rate under shear increases with increasing concentration of the MWNTs and the induction time for crystallization (defined as time at which the linear-viscoelastic properties commence to increase during a time sweep experiment) decreases with the increase of the concentration of MWNTs.

Further, no crystallization was observed with PBT nanocomposites samples containing graphite, sheared under similar conditions (Figure 5). This suggests that the crystallization kinetics and nucleating sites depend on the particle geometry and the corresponding surface/volume ratio. (For example, Byelov et al. have recently shown that particle shape can alter the flow field around the inclusion and lead to extra nucleating sites.[68]) The shear-induced crystallization from the melt should lead to increases in the number of affine junction points in the entangled polymer melt, to render the relaxation of the polymer segments and the backbone more difficult, thus increasing both the elasticity and the viscosity of the melt. The magnitude of the complex viscosity values of MWNT-PBT nanocomposites are orders of magnitude higher than those of the pure PBT and PBT suspensions containing graphite, indicating that the crystallinity that is induced due the presence of the MWNTs is significant (Figure 5). To gain insight to the effect of crystallization on changes in rheological behavior of the nanocomposite

Table 1. Melting Temperatures, Degree of Crystallinity, X_c, and Crystallization Temperatures of PBT and PBT Nanocomposites from DSC Analysis

sample	$T_{m,o}$ (°C)	$T_{m,p}$ (°C)	T_m (°C)	X_c (%)	$T_{c,o}$ (°C)	$T_{c,p}$ (°C)
pure PBT	208.6	227.2	238.4	20.7	191.3	173.3
0.5% MWNT-PBT	205.8	225.6	236	22.1	213.2	202.7
1% MWNT-PBT	205	228.6	235.8	22.9	214.2	204.4
2% MWNT-PBT	202.3	224.7	236.3	24.5	214.5	205.5

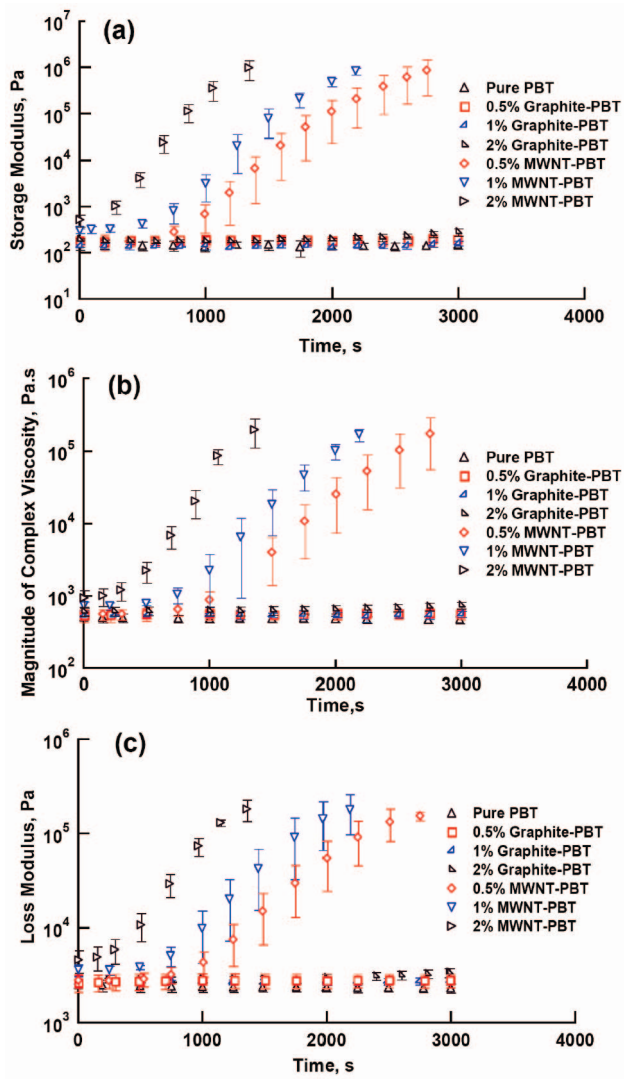

Figure 5. Variation of (a) storage modulus, (b) magnitude of complex viscosity, and (c) loss modulus with time at 1% strain, 5rps, 215 °C.

samples one can use the Krieger−Dougherty equation (eq 2) to represent the relative viscosity of a suspension, η_r, defined as the ratio of the shear viscosity of the suspension to the shear viscosity of the binder as a function of the volume fraction of rigid particles to account for the fraction of the volume immobilized due to crystallization over the maximum packing fraction ϕ_m (assumed to be 0.74 for face centered cubic):

$$\eta_r = \left(1 - \frac{\varphi}{\varphi_m}\right)^{-2.0} \tag{2}$$

Figure 6 shows the ratio of magnitude of complex viscosity of the nanosuspension over that of pure PBT versus shearing time for different loadings of MWNTs. The relative viscosity values reach 400−450 in 1325−1350 s of shearing. This suggests that on the basis of eq 2, the volume fraction of crystallites ϕ reaches about 0.7 in the same time period. This volume fraction approaches the maximum packing fraction, to give rise to crystalline morphologies that span the entire body of the nanosuspension constituting a gel-like or a solid-like structure. The absence of such shear-induced crystallization with the larger graphite particles (average particle size of graphite is 70 μm versus 10−30 nm for MWNTs) indicates that the change in the crystallization dynamics is significantly altered due to the availability of the very high surface area of MWNTs (90−350 m^2/g) to promote the crystallization of the polymer chains.

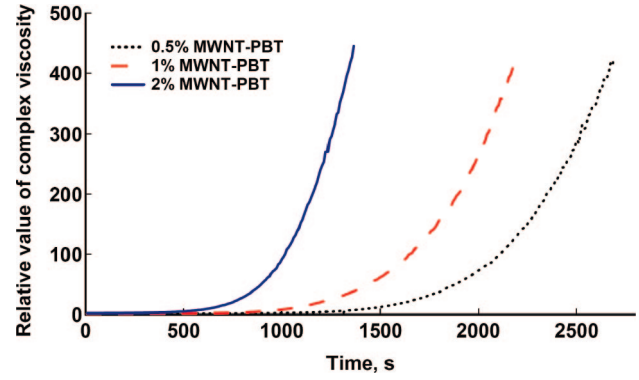

Figure 6. Ratio of the magnitude of complex viscosity of the nanosuspension over that of the pure polymeric binder versus shearing time for different loadings of MWNTs (at 1% strain, 5 rps, and 215 °C).

The mechanism for the crystallization of the nanocomposite at a temperature which is above the crystallization temperature of PBT should be associated with the nanoparticles serving as heterogeneous nucleating sites.[22,69−73] During heterogeneous nucleation the rate of nucleation is controlled by the availability and the concentration of the heterogeneous nuclei. Thus, the decrease of the induction time for shear-induced crystallization (as well as the noted crystallization under quiescent conditions discussed in section 3.1 with increased nanotube concentration) should be associated with an increase of the nucleation rate. Since such crystallization does not occur in the presence of larger carbon (graphite) particles, the observed changes in the crystallization behavior can be linked to the availability of the high surface area of the MWNTs to significantly increase the nucleation rate of PBT, as also noted earlier for the crystallization of MWNT incorporated PP under quiescent conditions.[28,54] Industrially, it has been known for some time that the compounding of particles with relatively small particle size into polymeric resins at relatively small concentrations changes the crystallization dynamics and the ensuing ultimate crystallinity/density distributions as well as altering the crystallite size and subsequently the mechanical properties of the polymer.[20]

From the results given in Figure 6, the significant level of crystallinity achieved upon shearing can be obtained at shorter durations by increasing the concentration of the MWNTs. For example, after approximately 1350s of shearing a relative viscosity of 9.5 is obtained for 0.5% by volume MWNTs, versus 46.7 for 1% by volume MWNTs and 445.2 for 2% by volume MWNTs. The reduced induction time with increasing concentration of MWNTs is again indicative of the important linkage between the initial concentration of the MWNTs acting as nucleating agents and the resulting nucleation/crystallization rate.

3.3. Effect of Applied Shear on PBT Nanocomposite Crystallization Rate. Figure 7 shows the time-dependent evolution of G', $|\eta^*|$, G'', and $\tan\delta = G''/G'$ of the 2% MWNT-PBT nanocomposite samples subjected to small-amplitude oscillatory shear at 215 °C and 1% strain amplitude at frequencies of 1, 3 and 5 rps. Consistent with the results shown in Figure 5, the pure PBT and the graphite-reinforced PBT samples did not show signs of shear-induced crystallization under these conditions (and thus were not included in Figure 7 for clarity). For the nanocomposite samples it is clearly observed that the crystallization rate increased and the induction time for crystallization decreased with increasing frequency. The work of de Gennes in dilute solutions of polymers has revealed that during flow the polymer chains undergo a step change from a random coil to a fully extended chain conformation at a critical

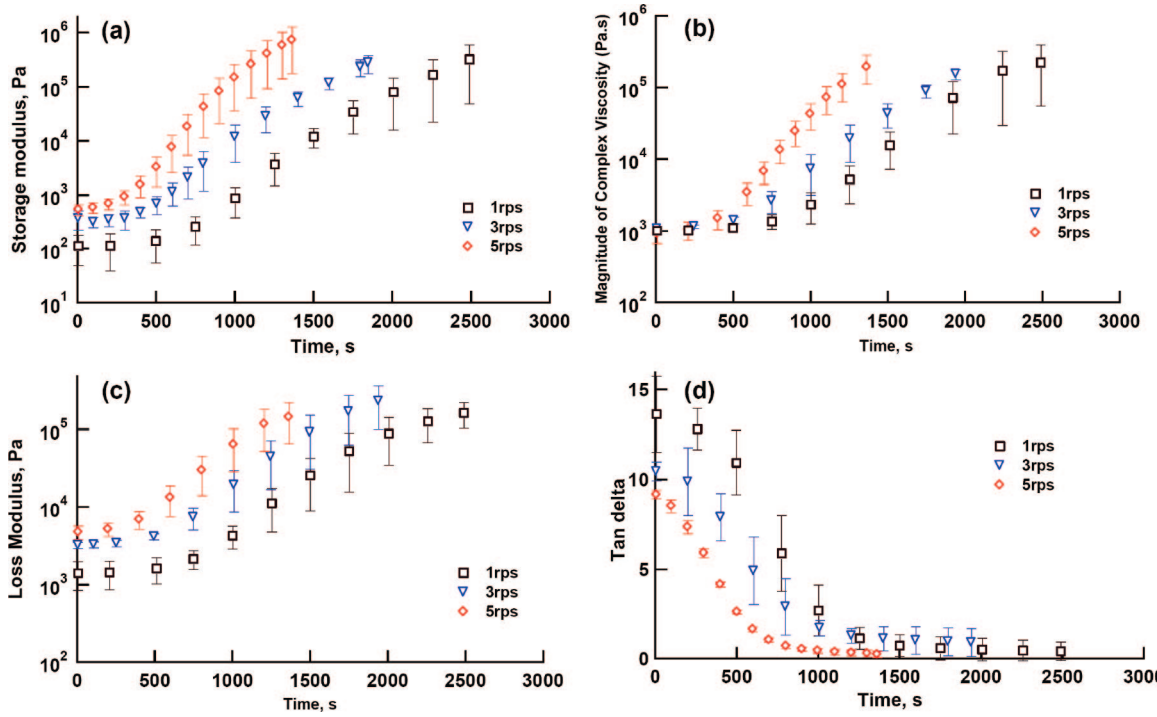

Figure 7. Variation of (a) storage modulus, (b) magnitude of complex viscosity, (c) loss modulus, and (d) tan δ with time for 2% MWNT-PBT at different frequencies (1% strain amplitude and 215 °C).

strain rate, without any intermediate stable chain conformations.[74] The subsequent studies of Keller et al. have provided experimental evidence to the occurrence of such a coil-stretch transition in macromolecules subject to crystallization under shear and extension on the basis of birefringence measurements, which exhibit an abrupt change as the strain rate is increased which is indicative of the formation of a fully extended chain conformation at the critical strain rate.[32,41] There is continuous stretching and relaxation of the macromolecules during shearing and the effect of nanotubes could be the prevention of the relaxation of the macromolecules.[30,75] Upon shear-induced crystallization the storage modulus, G', increases at a greater rate in comparison to the rate of increase of the loss modulus, G'', as a network structure associated with crystallization is developed (Figure 7d).

In our experiments, means to determine the degree of crystallinity as a function of time during the shear-induced crystallization process were not available. Instead, upon shearing at different durations of time the samples could be quenched at a constant rate of cooling to ambient temperature, followed by the determination of their degree of crystallinity to gain insight into the crystalline state formed during shear-induced crystallization. The percent crystallinity data associated with the samples sheared for different durations of time in the rheometer, followed by cooling under a constant cooling rate of 60 °C/min, are shown in Figure 8 for the 2% MWNT-PBT nanocomposite samples.

Figure 8 indicates that shearing the nanosuspensions at a relatively small deformation rate in the linear viscoelastic region is sufficient to increase the degree of crystallinity of PBT by about 33% (the degree of crystallinity of 2% MWNT-PBT increases from 24% to 32% upon shearing during crystallization versus crystallization under quiescent conditions). These results emphasize the important role played by the shearing process on the development of the crystallinity of the polymeric binder of the nanocomposite. They further suggest that the full potential of the MWNTs in altering/controlling the crystalline morphology of the polymer that they are incorporated into can

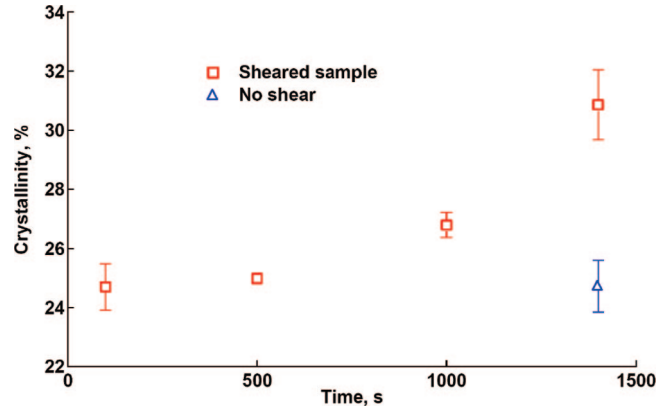

Figure 8. Effect of the duration of shearing on the degree of crystallinity values of 2% MWNT-PBT nanocomposites (following small-amplitude oscillatory shear at 1% strain, 5 rps, and 215 °C).

only be achieved upon subjecting the suspension to deformation during crystallization. Overall, the final morphology and crystallinity (and hence ultimate properties) of articles processed (molded/extruded) from nanocomposites are expected to be significantly affected by the thermo-mechanical history that the nanocomposite experiences during the processing operation. This is an important finding and could serve as the basis of new technologies associated with further enhancing/optimization of the properties of nanocomposites. Nanocomposite structures with significantly enhanced mechanical properties can be obtained by imposing high rates of shearing on the suspension during processing/shaping followed by rates of cooling which would prevent the relaxation of the macromolecules.

Figure 9 shows the typical results associated with shear-induced crystallization behavior of 2% MWNT-PBT nanocomposite samples characterized under differing strain amplitudes in the 1−5% range. The independence of the shear-induced crystallization behavior from the strain amplitude could have been anticipated, considering that these strain amplitudes are all in the linear viscoelastic range in which the structure of the

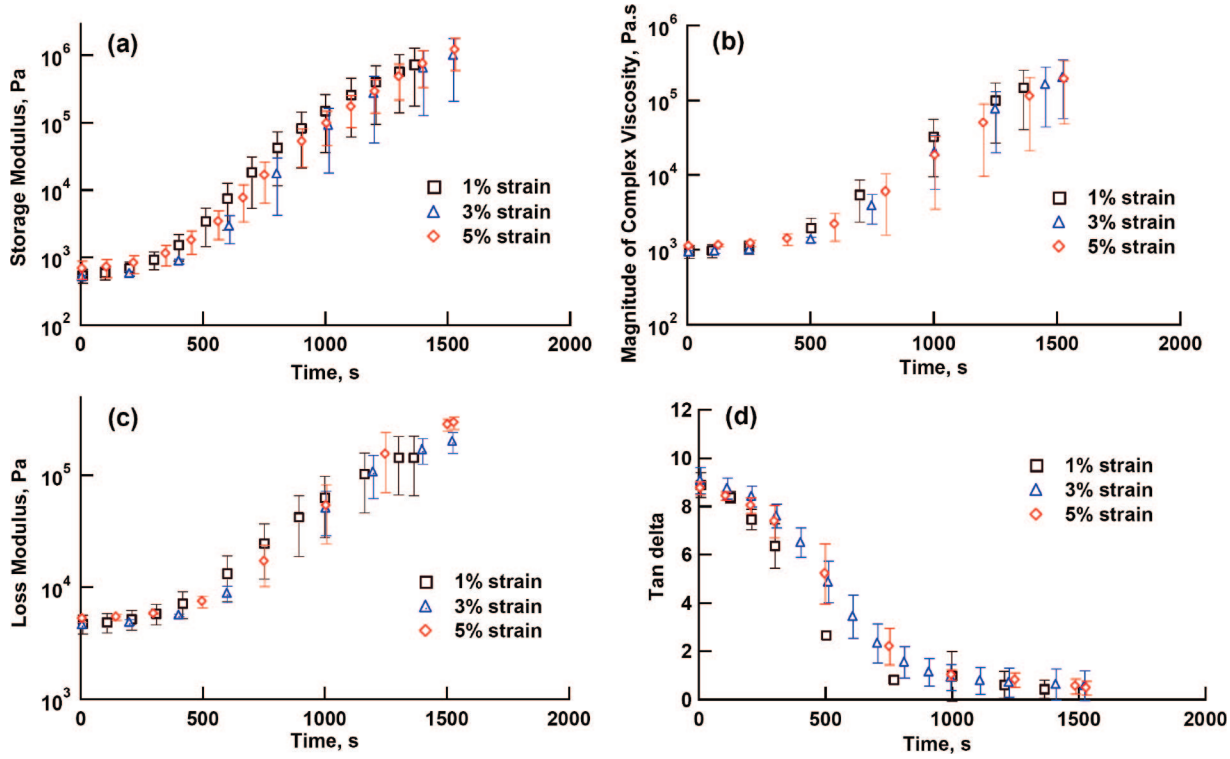

Figure 9. Variation of (a) storage modulus, (b) magnitude of complex viscosity, (c) loss modulus, and (d) tan δ with time for 2% MWNT-PBT at 1 rps, 215 °C as a function of different strain amplitudes.

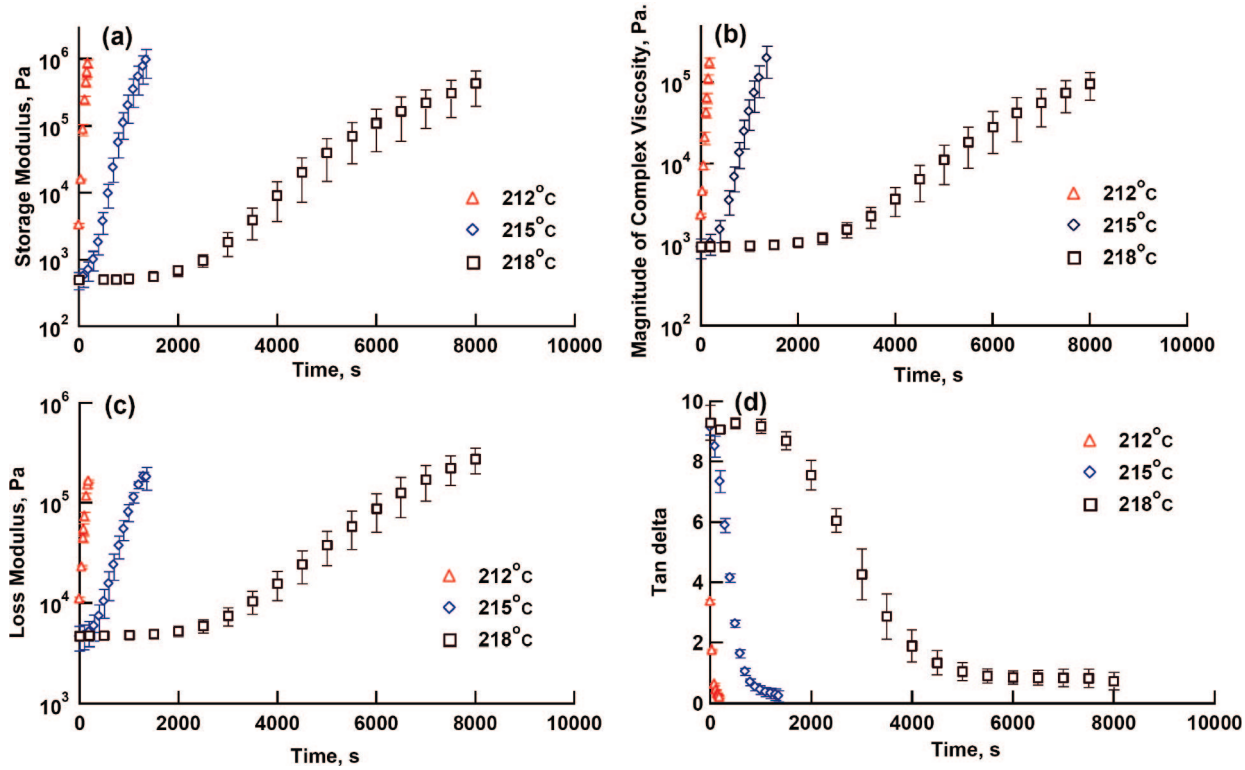

Figure 10. Variation of (a) storage modulus, (b) magnitude of complex viscosity, (c) loss modulus, and (d) tan δ with time for 2% MWNT-PBT at 1% strain, and 5 rps at different temperatures.

polymer melt is not far removed from its equilibrium entanglement state.

3.4. Effect of Temperature on Isothermal Crystallization Behavior of PBT Nanocomposites. Figure 10 shows the effects of temperature on the shear-induced crystallization behavior of 2% MWNT-PBT nanocomposites, subjected to oscillatory shear at 1% strain amplitude and 5 rps as a function of temperature. It can clearly be seen that the kinetics of the shear-induced crystallization process is affected by temperature.[61,62] Similar effects of temperature on crystallization kinetics have been observed under quiescent crystallization conditions.[70,76] Figure 10a indicates that the induction time for the onset of crystal-

Table 2. Young's Modulus and Crystallinity of PBT and PBT Nanocomposites Samples

sample	conditions	crystallinity (%)	Young's modulus (GPa)
pure PBT	no annealing	20.2	1.3
pure PBT	2 h annealed	27.3	1.7
pure PBT	5 h annealed	29.3	2.4
2% MWNT-PBT	no annealing	24.3	1.5
2% MWNT-PBT	sheared for 1365s	27.6	1.8

lization increases significantly with increasing temperature; for example, as the temperature is increased from 212 to 218 °C the induction time increases from 20 s to 2600 s. At the highest temperature imposed (218 °C), the rate of shear-induced crystallization is very slow and significant time needs to elapse for the crystallization process to initiate. Parts b and c of Figure 10 show the corresponding concomitant changes in the time-dependence of magnitude of complex viscosity and loss modulus with temperature. Overall, the rate of increase of the storage modulus with time is greater than that of the rate of increase of the loss modulus and eventually the tan delta values decrease to about one, suggesting again that a gel-like network, with the crystallites acting as network junction points, is formed.

3.5. Mechanical Properties. To understand the effect of polymer crystallinity on mechanical properties, pure PBT samples were annealed in a vacuum oven at 200 °C for periods of 2 and 5hrs, respectively. An increase in polymer crystallinity with annealing can be seen from Table 2. The results obtained for the pure PBT samples after annealing have been compared with both unsheared 2% MWNT-PBT and sheared 2% MWNT-PBT (sheared at 1% strain, 5 rps and 215 °C for 1365s) samples (see section 3.3 for details regarding collection of sheared and unsheared samples from ARES). As shown in Table 2, the presence of MWNTs as well as shearing increased the crystallinity of the PBT samples. It is well-known that changes in crystallinity affect the mechanical properties and permeability of the semicrystalline polymers.[33,57,77−79] It can be seen from Table 2 that the Young's modulus of pure PBT increased from 1.3 to 2.4 GPa as the crystallinity increased from 20.2 to 29.3% upon the annealing of the samples. Previous studies on PEEK and PBT have shown that the tensile strength at yield values increase and elongation at break values decrease with increasing crystallinity.[80,81] Overall, Table 2 suggests that the PBT samples with similar degrees of crystallinity also exhibit similar modulus values, indicating that annealing is as effective as the incorporation of 2% MWNTs in enhancing the modulus. The control of the modulus of the sheared samples should be affected by the preferred orientation of the MWNTs, a subject that is currently under investigation.

3.6. Avrami Equation and Crystallization Kinetics under Shear. The rate of crystallization data surmised from the monotonic increases of the dynamic properties with time during oscillatory shearing were used to analyze the kinetics of shearing under shear. Under quiescent conditions the kinetics of isothermal crystallization can be characterized using the Avrami equation[82]

$$X_c = 1 - \exp(-kt^n) \tag{3}$$

where X_c is the weight fraction crystallized at time t, k is the Avrami rate constant and n is the Avrami exponent. The Avrami exponent provides information on the nature of nucleation and growth processes during crystallization.[25,26] Note that in Eq 3 the parameters k and n are coupled. Thus a modified Avrami equation was used to remove this coupling[83,84]

$$X_c = 1 - \exp(-Kt)^n \tag{4}$$

where K is the composite Avrami rate constant, such that $k = K^n$. Using the modified Avrami equation the value of K (with units of inverse time) obtained using of eq 4 is independent of n.[83,84] A higher value of the Avrami exponent is indicative of the state of preferred orientation of the polymer chains during the crystallization process and the resulting increase in the nucleation and growth rates.

Table 3. Kinetic Parameters of the Avrami Equation for Different Loadings of MWNTs in PBT Nanocomposites Sheared at 1% Strain and 5 rps at 215°C

MWNT loading (vol %)	Avrami constant, K (s^{-1})	Avrami exponent, n
0		
0.5	0.00062	8.0
1.0	0.00078	7.4
2.0	0.0012	6.5

Table 4. Kinetic Parameters of the Avrami Equation as a Function of Temperature for 2% MWNT-PBT Sheared at 1% Strain and 5 rps

Temperature (°C)	Avrami constant, K (s^{-1})	Avrami exponent, n
212	0.0085	6.1
215	0.0012	6.5
218	0.0002	6.7

Flory theory suggests that the storage modulus would be proportional to the degree of cross-linking,[85] and hence crystallization from the melt can be considered to be akin to the development of a network structure with the crystallites acting as cross-links/junction points. Thus the change in the storage modulus during the shear-induced crystallization process can be taken to be indicative of the rate of crystallization on the basis of a normalized modulus, $G_n(t)$:

$$G_n(t) = \frac{G'(t) - G'(0)}{G'(\infty) - G'(0)} \tag{5}$$

where $G'(t)$ is the storage modulus at time t, $G'(0)$ is the storage modulus at t=0 and the $G'(\infty)$ is the storage modulus value at the conclusion of the shearing process.[86] In our rheometry experiments the time during shear-induced crystallization at which the torque and normal force transducers are overloaded (i.e., the torque and normal force values surpass the maximum allowable limits of the force and torque transducers, approximately 1000 g-cm) is the point that the shear-induced crystallization experiment is terminated. It is assumed that this state of torque/normal force overload represents the ultimate $G'(\infty)$ value. Using this normalized modulus, an Avrami-type equation for the normalized storage modulus can be written as

$$G_n(t) = 1 - \exp(-Kt)^n \tag{6}$$

From eqs 5 and 6, the kinetic parameters of the Avrami equation (the exponent n and the crystallization rate constant K) can be obtained from the slope and the intercept of a plot of $\log [-\ln(1 - G_n(t))]$ versus $\log t$, respectively.

As shown in Tables 3 and 4, the value of K increases upon the incorporation of MWNTs and upon the decrease of the temperature at which shearing occurs, reflecting the faster rate of PBT crystallization in the presence of MWNTs and with decreasing temperature. Such increases in the value of K were also observed upon the incorporation of glass fibers to PBT[22] as well as upon decreasing the temperature employed during quiescent crystallization conditions for nanocomposites of poly(propylene)[54,69] and high density polyethylene.[70] Tables 3 and 4 show that the values of the Avrami exponent n are significantly higher (6.5−8.0) than those encountered during crystallization of macromolecular melts under quiescent conditions, where n typically lies between 2 and 4. The higher values of the Avrami exponent can be considered to be a reflection of the different mechanism of crystallization associated with shear-induced crystallization versus crystallization under quiescent

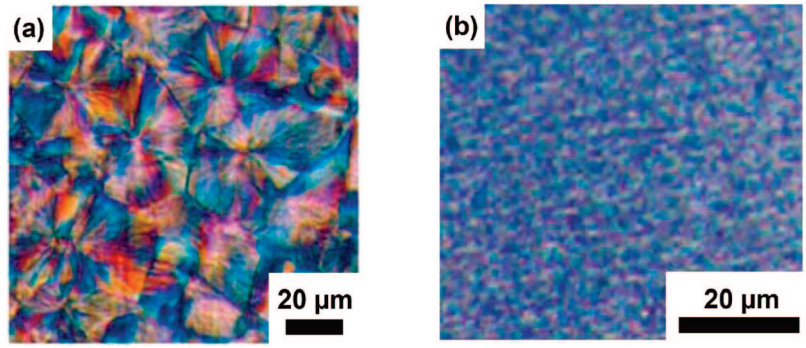

Figure 11. Polarized light microscopy images of (a) pure PBT and (b) 0.5% MWNT-PBT nanocomposite samples crystallized under quiescent (no shear) conditions.

conditions.[87−89] Under flow-induced conditions, the polymer chains orient (and stretch) in the direction of shear, with concomitant crystallization of the macromolecules occurring on the surfaces of the nanotubes to accelerate the crystallization process. This we believe is the underlying reason for the higher values of the Avrami exponent associated with shear-induced crystallization versus those determined under quiescent conditions. While the Avrami exponent slightly decreases with the increase of the MWNT concentration and decrease of the temperature, the fact that the values of n remain in a narrow range suggests that the mechanism of shear-induced crystallization remains the same regardless of the concentration of the MWNTs and the temperature.

3.7. Morphology of PBT and PBT Nanocomposites. Specimens of pure PBT and melt-mixed nanocomposite samples of PBT with 0.5% (by volume) of MWNT crystallized under quiescent conditions were subjected to additional microstructural analysis employing polarized microscopy. The effect of the incorporation of the MWNTs on PBT spherulite size for samples crystallized under quiescent conditions can be seen very clearly from the images shown in Figure 11. Upon the incorporation of MWNTs the spherulite sizes of PBT decreased from approximately 20−50 μm to around 1−5 μm. The crystallite size is controlled by the number of nuclei present, since the spherulites only continue to grow until they impinge on each other. With a greater number of nuclei present due to the MWNTs acting as heterogeneous nuclei, the eventual diameters of the spherulites should decrease as indeed shown in Figure 11.

To elucidate the effects of shearing on the development of the crystalline morphology, sheared nanocomposite samples (0.5% MWNT-PBT) were also analyzed using polarized microscopy (not shown). The sizes of spherulites of specimens obtained upon shear-induced crystallization appeared to be even smaller than those crystallized under quiescent conditions. This suggests that shearing further increases the rate of nucleation, possibly by increasing the frequency of the contacts between the macromolecules and the nanotubes on one hand and preventing the relaxation of stretched macromolecules on the other. These results also contribute to the body of evidence indicating that the significant changes in mechanical properties observed when relatively small concentrations of nanoparticles are compounded into polymeric resins are linked to the effects of the incorporation of nanoparticles on the dynamics of the nucleation and growth rates during crystallization. Generally, the decrease of the crystallite size (as noted here due to the effect of shearing on the crystallization process) is expected to lead to superior mechanical properties as noted earlier for injection moldings of polyethylene resins.[20]

To gain further insight into the structure of the shear-induced crystallites, fuming nitric acid was used to etch the amorphous phase of the sheared 0.5% MWNT-PBT nanocomposite samples for subsequent SEM analysis, following the procedures suggested in earlier studies.[90−93] Figure 12 shows the crystal structure of the 0.5% MWNT-PBT sample (sheared for 2800 s at 1% strain amplitude and 5rps at a temperature of 215 °C). The spherulites of PBT appear to have a fairly uniform size of around 1.5−3 μm upon shearing and are smaller than the spherulites that form upon crystallization from quiescent conditions (4−5 μm) (Figure 11(b)). It is likely that the PBT spherulites are clustered along the length of MWNTs, which themselves could be flocculated to some degree and preferentially oriented along the flow streamlines during simple shearing.

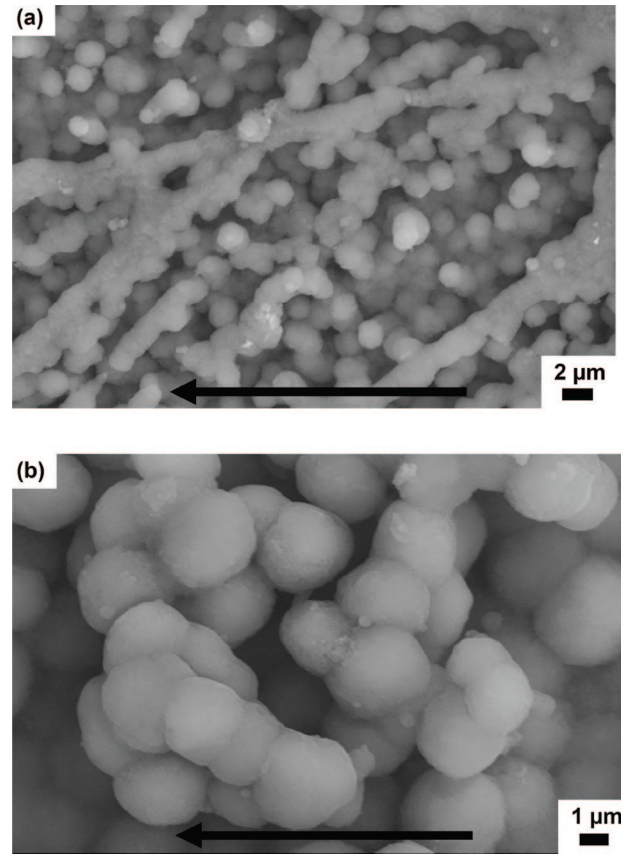

Figure 12. SEM images showing the effect of shearing on the morphology of 0.5% MWNT-PBT nanocomposites sheared at 1% strain amplitude, 5 rps, and 215 °C: (a) low magnification; (b) high magnification. Arrows indicate the approximate flow direction.

The orientation direction of the crystal clusters (the typical lengths of the MWNTs are in the range of 1−10 μm) appears to coincide with the flow direction as shown in Figure 12a. The clustering of the spherulitic morphologies are better seen in

Figure 12b with some degree of preferred orientation of the clusters along the direction of the oriented backbones of MWNT (single or floccules of MWNTs). For various types of semicrystalline polymers, including polyethylene and polyamide 6,6, it is documented that crystals indeed start growing perpendicular to the surfaces of the nanotubes resulting in nanohybrid shish-kebab (NHSK) structures.[30,94−96] Here upon the nucleation of multiple polymer chains on any nanotube surface, spherulitic morphologies that cover the surface of the nanotube appear to have developed. The nanotubes are not visible upon etching, presumably upon their coverage with the PBT crystals. The formation of crystalline layering on the surfaces of nanotubes has been observed by others.[97]

4. Conclusions

This study further adds to the body of evidence that suggests that the significant changes in ultimate properties (mechanical, permeability, etc.) of multiwalled carbon nanotube-incorporated polymers can be to some degree associated with the changes in the degree of crystallinity and the crystalline morphologies induced by the presence of MWNTs, occurring on the basis of the high surface to volume ratios of MWNTs. Shearing promotes the crystallization of the PBT in the presence of MWNTs giving rise to a significant increase of the degree of crystallinity. These results further suggest that the thermo-mechanical history that the nanocomposite is exposed to during processing is a key determinant in the development of the structure and the ultimate properties of the nanocomposite. Thus conditions that promote shear-induced crystallization (deformation rate, time, temperature, etc) can provide the means to increase the overall crystallinity, decrease the crystallite sizes and alter the crystalline morphology within the nanocomposite samples, all of which could be exploited as a means to tailor the properties of processed nanocomposite samples.

References and Notes

(1) Kharchenko, S. B.; Douglas, J. F.; Obrzut, J.; Grulke, E. A.; Migler, K. B. *Nat. Mater.* **2004**, *3*, 564.
(2) Koerner, H.; Price, G.; Pearce, N. A.; Alexander, M.; Vaia, R. A. *Nat. Mater.* **2004**, *3*, 115.
(3) Miaudet, P.; Derre, A.; Maugey, M.; Zakri, C.; Piccione, P. M.; Inoubli, R.; Poulin, P. *Science* **2007**, *318*, 1294.
(4) Pasquali, M. *Nat. Mater.* **2004**, *3*, 509.
(5) Shaffer, M. S. P.; Windle, A. H. *Adv. Mater.* **1999**, *11*, 937.
(6) Shah, D.; Maiti, P.; Gunn, E.; Schmidt, D. F.; Jiang, D. D.; Batt, C. A.; Giannelis, E. P. *Adv. Mater.* **2004**, *16* (14), 1173.
(7) Dang, Z.; Wang, L.; Yin, Y.; Zhang, Q.; Lei, Q. *Adv. Mater.* **2007**, *19*, 852.
(8) Mago, G.; Kalyon, D. M.; Fisher, F. T. *J. Nanomater.* **2008**, Vol. 2008, Article ID 759825, 8.
(9) Vigolo, B.; Penicaud, A.; Coulon, C.; Sauder, C.; Pailler, R.; Journet, C.; Bernier, P.; Poulin, P. *Science* **2000**, *290*, 1331.
(10) White, J. L.; Potente, H., *Screw Extrusion*; Hanser Publishers: Munich, Germany, 2003.
(11) Demirkol, E.; Kalyon, D. M. *J. Appl. Polym. Sci.* **2007**, *104*, 1391–1398.
(12) Erol, M.; Kalyon, D. M. *Int. Polym. Process.* **2005**, *20*, 228–237.
(13) Feber, C.; Gelome, J. D.; Mcglashan-Powell, M.; Kalyon, D. M. *IBM J. Res. Dev.* **2005**, *49* (4/5), 699–707.
(14) Kalyon, D. M.; Birinci, E.; Yazici, R.; Karuv, B.; Walsh, S. *Polym. Eng. Sci.* **2002**, *42*, 1609–1617.
(15) Kalyon, D. M.; Dalwadi, D.; Erol, M.; Birinci, E.; Tsenoglu, C. *Rheol. Acta* **2006**, *45*, 641–658.
(16) Kalyon, D. M.; Gevgilili, H.; Shah, A. *Int. Polym. Process.* **2004**, *19*, 129–138.
(17) Keller, A.; Kolnaar, H. *Processing of Polymers*; Wiley-VCH: New York, 1997; Vol. *18*, p 189.
(18) Malik, M.; Kalyon, D. M. *Int. Polym. Process.* **2005**, *20*, 398–409.
(19) Tadmor, Z.; Gogos, C. *Principles of Polymer Processing*, 2nd ed.; Wiley: New York, 2007.
(20) Kamal, M. R.; Kalyon, D. M.; Dealy, J. *Polym. Eng. Sci.* **1980**, *20*, 1117–1126.
(21) Degirmenbasi, N.; Ozkan, S.; Kalyon, D. M.; Yu, X. *J. Biomed. Mater. Res. A* **2008**, on-line.
(22) Park, C.; Lee, K.; Nam, J.; Kim, S. *J. Appl. Polym. Sci.* **2000**, *78*, 576–585.
(23) Cebe, P.; Hong, S. *Polymer* **1986**, *27*, 1183–1986.
(24) Velisaris, C. N.; Seferis, J. C. *Polym. Eng. Sci.* **1986**, *26*, 1574–1581.
(25) Kamal, M. R.; Chu, E. *Polym. Eng. Sci.* **1983**, *23*, 27–31.
(26) Supaphol, P.; Spruiell, J. E. *J. Appl. Polym. Sci.* **2000**, *75*, 44–59.
(27) Baughman, R. H.; Zakhidov, R. H.; de Heer, W. A. *Science* **2002**, *297*, 787.
(28) Assouline, E.; Lustiger, A.; Barber, A. H.; Cooper, C. A.; Klein, E.; Wachtel, E.; Wagner, H. D. *J. Polym. Sci., Part B: Polym. Phys.* **2003**, *41*, 520–527.
(29) Coleman, J. N.; Khan, U.; Gun'ko, Y. K. *Adv. Mater.* **2006**, *18*, 689–706.
(30) Garcia-Gutierrez, M. C.; Hernandez, J. J.; Nogales, A.; Panine, P.; Rueda, D. R.; Ezquerra, T. A. *Macromolecules* **2008**, *41* (3), 844–851.
(31) Mago,G.; Fisher, F. T.; Kalyon, D. M. *J. Nanosci. Nanotechnol.* **2008**, in press.
(32) Bashir, Z.; Odell, J. A.; Keller, A. *J. Mater. Sci.* **1986**, *21*, 3993–4002.
(33) Bigg, D. M. *Polym. Eng. Sci.* **1988**, *28*, 830.
(34) Cabarcos, E. L.; Bayer, R. K.; Zachmann, H. G. *Polym. Eng. Sci.* **1989**, *29* (3), 193.
(35) Clark, E. S.; Garber, C. A. *Int. J. Polym. Mater.* **1971**, *1*, 31–46.
(36) Kakiage, M.; Sekiya, M.; Yamanobe, T.; Komoto, T.; Sasaki, S.; Murakami, S.; Uehara, H. *Polymer* **2007**, *48*, 7385–7392.
(37) Lee, O.; Kamal, M. R. *Polym. Eng. Sci.* **1999**, *39* (2), 236.
(38) McHugh, A. J. *Polym. Eng. Sci.* **1982**, *22* (1), 15.
(39) Lu, F.; Spruiell, J. E. *J. Appl. Polym. Sci.* **1986**, *31*, 1595–1607.
(40) Binsbergen, F. L. *Nature* **1966**, *211*, 516.
(41) Keller, A.; Machin, M. J. *J. Macromol. Sci. (Phys.)* **1967**, *1*, 41–91.
(42) Mackley, M. R.; Frank, F. C.; Keller, A. *J. Mater. Sci.* **1975**, *10*, 1501–1509.
(43) Monks, A. W.; White, H. M.; Bassett, D. C. *Polymer* **1996**, *37*, 5933–5936.
(44) Somani, R. H.; Yang, L.; Zhu, L.; Hsiao, B. S. *Polymer* **2005**, *46*, 8587–8623.
(45) McHugh, A. J. *J. Appl. Polym. Sci.* **1975**, *19*, 125–140.
(46) McHugh, A. J.; Doufas, A. K. *Composites: Part A* **2001**, *32*, 1059–1066.
(47) de Gennes, P. G. *Langmuir* **2002**, *18*, 3413–3414.
(48) Denn, M. *Annu. Rev. Fluid Mech.* **2001**, *33*, 265–287.
(49) Kalyon, D. M.; Gevgilili, H. *J. Rheol.* **2003**, *47*, 683.
(50) Kalyon, D. M. *J. Rheol.* **2005**, *49*, 621–640.
(51) Tang, H. S.; Kalyon, D. M. *J. Rheol.* **2008**, *52* (2), 507.
(52) Aral, B. K.; Kalyon, D. M. *J. Rheol.* **1994**, *38* (4), 957.
(53) Illers, K. H. *Colloid Polym. Sci.* **1980**, *258*, 117–124.
(54) Bhattacharya, A. R.; Sreekumar, T. V.; Liu, T.; Kumar, S.; Ericson, L.; Hauge, R.; Smalley, R. E. *Polymer* **2003**, *44*, 2373–2377.
(55) Valentini, L.; Biagiotti, J.; Lopez-Manachado, M. A.; Santucci, S.; Kenny, J. M. *Polym. Eng. Sci.* **2004**, *44*, 303–311.
(56) Lee, J. H.; Park, T. G.; Park, H. S.; Lee, D. S.; Lee, Y. K.; Yoon, S. C.; Nam, J. *Biomaterials* **2003**, *24*, 2773.
(57) Sandler, J.; Windle, A. H.; Werner, P.; Altstadt, V.; Es, M. V.; Shaffer, M. S. P. *J. Mater. Sci.* **2003**, *38*, 2135–2141.
(58) Ryan, K. P.; Cadek, M.; Nicolosi, V.; Walker, S.; Ruether, M.; Fonseca, A.; Nagy, J. B.; Coleman, J. N. *Synth. Met.* **2006**, *156*, 332–335.
(59) Kim, J. Y.; Park, H. S.; Kim, S. H. *Polymer* **2006**, *47*, 1379–1389.
(60) Cadek, M.; Coleman, J. N.; Barron, V.; Hedicke, K.; Blau, W. J. *Appl. Phys. Lett.* **2002**, *81*, 5123.
(61) Chien, M. C.; Weiss, R. A. *Polym. Eng. Sci.* **1988**, *28*, 6–9.
(62) Myung, H. S.; Yoon, M. J.; Yoo, E. S.; Kim, B. C.; Im, S. S. *J. Appl. Polym. Sci.* **2001**, *80*, 2640–2646.
(63) Carrot, C.; Guillet, J.; Boutahar, K. *Rheol. Acta* **1993**, *32*, 566–574.
(64) Pennings, A. J. *J. Cryst. Growth* **1980**, *48*, 574–581.
(65) Pennings, A. J.; Lageveen, R.; De Vries, R. S. *Colloid Polym. Sci.* **1977**, *255*, 532–542.
(66) Pennings, A. J.; Zwijnenburg, A.; Lageveen, R. *Colloid Polym. Sci.* **1973**, *251*, 500–501.
(67) Zwijnenburg, A.; Pennings, A. J. *Colloid Polym. Sci.* **1976**, *254*, 868–881.
(68) Byelov, D.; Panine, P.; Remerie, K.; Biemond, E.; Alfonso, G. C.; de Jeu, W. H. *Polymer* **2008**, *49*, 3076–3083.
(69) Grady, B. P.; Pompeo, F. P.; Shambaugh, R. L.; Resasco, D. E. *J. Phys. Chem. B* **2002**, *106*, 5852–5858.
(70) Haggenmueller, R.; Fischer, J. E.; Winey, K. I. *Macromolecules* **2006**, *39*, 2964–2971.
(71) Minus, M. L.; Chae, H. G.; Kumar, S. *Polymer* **2006**, *47*, 3705–3710.
(72) Moniruzzaman, M.; Winey, K. I. *Macromolecules* **2006**, *39*, 5194–5205.
(73) Probst, O.; Moore, E. M.; Resasco, D. E.; Gardy, B. P. *Polymer* **2004**, *45*, 4437–4443.

(74) De Gennes, P. G. *J. Chem. Phys.* **1974**, *60*, 5030.
(75) Li, L.; De Jeu, W. H. *Macromolecules* **2004**, *37*, 5646–5652.
(76) Li, L.; Li, C. Y.; Ni, C.; Rong, L.; Hsiao, B. S. *Polymer* **2007**, *48*, 3452–3460.
(77) Polyakova, A.; Stepanov, E. V.; Sekelik, D.; Schiraldi, D. A.; Hiltner, A.; Baer, E. *J. Polym. Sci., Part B: Polym. Phys.* **2001**, *39*, 1911–1919.
(78) Qureshi, N.; Stepanov, E. V.; Schiraldi, D.; Hiltner, A.; Baer, E. *J. Polym. Sci., Part B: Polym. Phys.* **2000**, *38*, 1679–1686.
(79) Busick, D. N.; Spontak, R. J.; Balik, C. M. *Polymer* **1999**, *40*, 6023–6029.
(80) Cebe, P.; Chung, S. Y.; Hong, S. *J. Appl. Polym. Sci.* **1987**, *33*, 487–503.
(81) Mago, G.; Dutreuil, J.; Fisher, F. T.; Kalyon, D. M. ASME-IMECE 2007 Conference Proceedings, Seattle, WA.
(82) Avrami, M. *J. Chem. Phys.* **1939**, 1103–1112.
(83) Khanna, Y. P.; Taylor, T. J. *Polym. Eng. Sci.* , *28*, 1042–1045.
(84) Supaphol, P.; Dangseeyun, N.; Srimoaon, P.; Nithitanakul, M. *Thermochim. Acta* **2003**, *406*, 207–220.
(85) Flory, P. J. *Principles of Polymer Chemistry*; Cornell University Press: Ithaca, NY, 1953.
(86) Khanna, Y. P. *Macromolecules* **1993**, *26*, 3639–3643.
(87) Wunderlich, B., *Macromolecular Physics*; Academic Press, Inc.: New York, 1976; Vol. *2*, pp 216−232.
(88) Sherwood, C. H.; Price, F. P.; Stein, R. S. *J. Polym. Sci.: Polym. Symp.* **1978**, *63*, 77–94.
(89) Fritzsche, A. K.; Price, F. P.; Ulrich, R. D. *Polym. Eng. Sci.* **1976**, *16* (3), 182.
(90) Blundell, D. J.; Crick, R. A.; Fife, B.; Peacock, J.; Keller, A.; Waddon, A. *J. Mater. Sci.* **1989**, *24*, 2057–2064.
(91) Chang, E. P.; Slagowski, E. L. *J. Appl. Polym. Sci.* **1978**, *22*, 769–779.
(92) Lopez, L. C.; Wilkes, G. L. *J. Polym. Sci.: Polym. Lett.* **1986**, *24*, 573–579.
(93) Shahin, M. M.; Olley, R. H. *J. Polym. Sci., Part B: Polym. Phys.* **2002**, *40*, 124–133.
(94) Kodjie, S. L.; Li, L.; Li, B.; Cai, W.; Li, C. Y.; Keating, M. *J. Macromol. Sci., Part B: Phys.* **2006**, *45*, 231–245.
(95) Li, C. Y.; Li, L.; Cai, W.; Kodjie, S. L.; Tenneti, K. K. *Adv. Mater.* **2005**, *17*, 1198–1202.
(96) Yue, J.; Xu, Q.; Zhang, Z.; Chen, Z. *Macromolecules* **2007**, *40*, 8821–8826.
(97) Zhang, S.; Minus, M. L.; Zhu, L.; Wong, C. P.; Kumar, S. *Polymer* **2008**, *49*, 1356–1364.

MA8008838